A) Supersolidity in Hard-Core-Boson (HCB) systems

Understanding the microscopic mechanism of coexisting long-range orders (such as lattice supersolidity) in naturally occurring and artificially designed strongly correlated systems has been and will continue to be an area of immense interest. While phenomenological pictures exist to explain lattice-supersolidity, a microscopic theory that elucidates the homogeneous coexistence is yet to be formulated.

We study lattice systems of HCBs strongly-coupled to optical phonons. *Devising a strong-weak duality treatment, we map strong-coupling problems (in the original frame of reference) to weak-coupling problems (in the dual frame of reference) with the small parameter being the inverse of that in the original frame of reference*. Our duality treatment is potentially employable in various fields of physics dealing with strong coupling between fermions/HCBs and massive bosonic excitations (such as optical phonons, plasmons, etc.). In the dual frame of reference, effective Hamiltonians are derived using perturbation theory. The effective Hamiltonians (for HCBs strongly-coupled to optical phonons) belong to the class of extended boson Hubbard models of the type $\mathbf{t_1}$-$\mathbf{t_2}$-....-$\mathbf{t_m}$-$\mathbf{V_1}$-$\mathbf{V_2}$-....-$\mathbf{V_n}$ [involving hoppings $\mathbf{t_1}$, $\mathbf{t_2}$, $\mathbf{t_3}$, etc. and interactions $\mathbf{V_1}$, $\mathbf{V_2}$, $\mathbf{V_3}$, etc. of ranges nearest neighbor (NN), next-nearest neighbor (NNN), next-to-next-nearest neighbor (NNNN), etc.]. Unlike many lattice models of the extended boson Hubbard type, the parameters (i.e., hopping term, strength of HCB-phonon coupling, and phonon frequency) in our $\mathbf{t_1}$-$\mathbf{t_2}$-....-$\mathbf{t_m}$-$\mathbf{V_1}$-$\mathbf{V_2}$-....-$\mathbf{V_n}$ model either can be determined from band-structure calculations or can be obtained from experiments. It is important to point out that our derivations [see Sanjoy Datta, Arnab Das, and Sudhakar Yarlagadda, Phys. Rev. B, **71** 235118 (2005) and later works] also correct the oversight in the effective Hamiltonian (obtained from a different approach for the one-dimensional Holstein Model) reported in the well-cited work of Jorge E. Hirsch and Eduardo Fradkin, Phys. Rev. B **27**, 4302 (1983).

The minimum model for realizing a checkerboard supersolid (**cSS**) is shown to be the $\mathbf{t_2}$-$\mathbf{V_1}$ model. On the other hand, $\mathbf{t_1}$-$\mathbf{V_1}$-$\mathbf{V_2}$-$\mathbf{V_3}$ model is demonstarted to be the minimum model for obtaining a rare diagonal striped supersolid (**dsSS**). The mechanism governing the existence of a supersolid phase away from commensurate fillings, on unfrustrated system (such as the square lattice), is that interstitials or vacancies can move without a cost in the potential energy; however, importantly, particles on the crystal lattice also take part in the superflow.

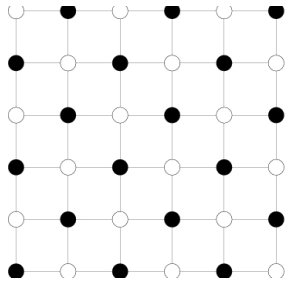

(a)

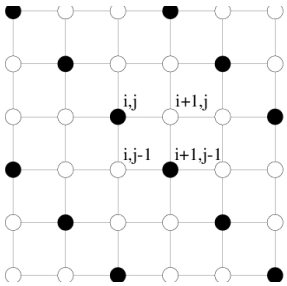

(b)

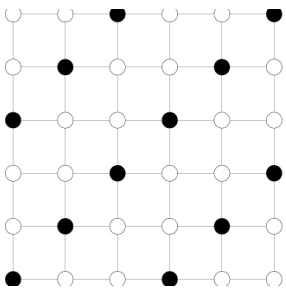

(c)

FIG. 1. Different types of CDWs: (a) checkerboard solid (**cS**) at half-filling with S(**Q**) peaking at **Q** =(π,π); (b) diagonal striped solid (**dsS**) indicated by peak in S(**Q**) at **Q**=(2π/3,2π/3); and (c) **dsS** characterized by ordering wavevector **Q** = (2π/3,4π/3).

A.1) Checkerboard-supersolidity in a two-dimensional Bose-Holstein model

Satyaki Kar and Sudhakar Yarlagadda, Annals of Physics **375**, 322 (2016).

Here we study the cooperation/competition of the superfluid and charge-density-wave (CDW) orders in a two-dimensional Bose-Holstein model where HCBs are coupled locally to optical phonons. In the parameter regimes of strong HCB-phonon coupling and nonadiabaticity, we find a novel mechanism for lattice-supersolidity (namely, sizeable same-sublattice tunneling in presence of large nearest-neighbor repulsion) in the system. The ground state phase diagram is obtained using Quantum Monte Carlo simulation involving stochastic-series-expansion technique. At densities not far from half filling and in the parameter regime where the double-hopping terms are non-negligible (negligible) compared to the nearest-neighbor hopping, we get checkerboard-supersolidity (phase separation) with CDW being characterized by ordering wavevector **Q** = (π,π).

The following effective $\mathbf{t_1\text{-}t_2\text{-}t_3\text{-}V_1}$ Hamiltonian for the HCB particles on a 2D square lattice is obtained:

$$H_e = - g^2 \omega_0 \sum_j n_j - t_1 \sum_{j,\delta} b_j^\dagger b_{j+\delta} - t_2 \sum_{j,\delta'} b_j^\dagger b_{j+\delta'} - t_3 \sum_{j,\delta''} b_j^\dagger b_{j+\delta''}$$

$$- V_1/2 \sum_{j,\delta} n_j (1- n_{j+\delta}) \qquad (1)$$

where δ' and δ'' denote next-nearest-neighbor (NNN) and next-to-next-nearest neighbor (NNNN) sites respectively; $t_1 = t \exp(-g^2)$, $t_2 = 2t^2 \exp(-g^2)/(g^2\omega_0)$, $t_3 = t_2/2$, and $V_1 \sim t^2/(g^2\omega_0)$

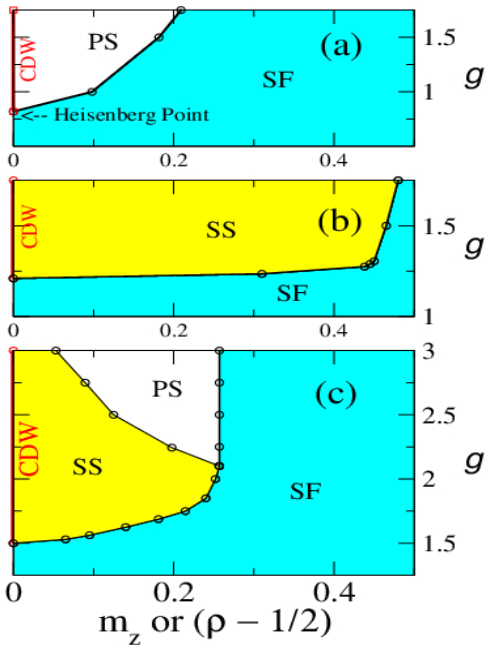

FIG. 2. Quantum phase diagrams at various magnetizations $\mathbf{m_z}$ (or fillings ρ) and

HCB-phonon coupling g when adiabaticity $t/\omega_0 = 1.0$. The calculations are for a 16X16 lattice and for our BH system [using Eq. (1)] by (a) considering interaction and only nearest-neighbor hopping, i.e., $t_2 = t_3 = 0$; (b) setting $t_1 = 0$, i.e., considering interaction and only NNN and NNNN hoppings; and (c) including interaction and and all the hoppings. Here PS, SS, and SF refer to Phase Separation, Supersolid, and Superfluid.

A.2) An analysis of the t_2 -V model

Amrita Ghosh and Sudhakar Yarlagadda, Phys. Rev. B **90**, 045140 (2014).

Some time ago, we derived the effective Hamiltonian for the cooperative electron-phonon interaction (EPI) quantum systems in one-dimension [R. Pankaj and S. Yarlagadda, PRB **86**, 035453 (2012)]; it has been demonstrated analytically that introducing cooperative effects in the strong EPI limit changes the dominant transport mechanism from one of nearest-neighbor (NN) hopping to that of next-nearest-neighbor (NNN) hopping. Additional NN particle repulsion (due to incompatibility of distortions produced by cooperative EPI effects) leads to the $\mathbf{t_1}$-$\mathbf{t_2}$-$\mathbf{V_1}$ model as the effective model. Recently (after us) T. Mishra, R. V. Pai, and Subroto Mukerjee [PRA **89**, 013615 (2014)] studied the $\mathbf{t_1}$-$\mathbf{t_2}$-$\mathbf{V_1}$ model.

We study a novel model (i.e., the $\mathbf{t_2}$-$\mathbf{V_1}$ model involving next-nearest-neighbor hopping and nearest-neighbor repulsion) in one dimension that generically depicts the dominant transport mechanism in cooperative strong electron-phonon interaction systems. Using analytic and numerical approaches, hard-core bosons are shown to typically undergo a striking discontinuous transition from a superfluid to a supersolid. Topological inequivalence of rings with even and odd number of sites is manifested through observable differences (in structure factor peaks) at the transition. Connections are also identified between the $\mathbf{t_2}$-$\mathbf{V_1}$ model and other topologically interesting models.

The above work (on the $\mathbf{t_2}$-$\mathbf{V_1}$ model) has been used/extended by X. Huo, Y.-Y. Cui, D. Wang, and J.-P. Lv, Phys. Rev. A **95**, 023613 (2017); T. Bilitewski and N. R. Cooper Phys. Rev. A **94**, 023630 (2016); R. W. Chhajlany, P. R. Grzybowski, J. Stasinska, M. Lewenstein, and O. Dutta Phys. Rev. Lett. **116**, 225303 (2016).

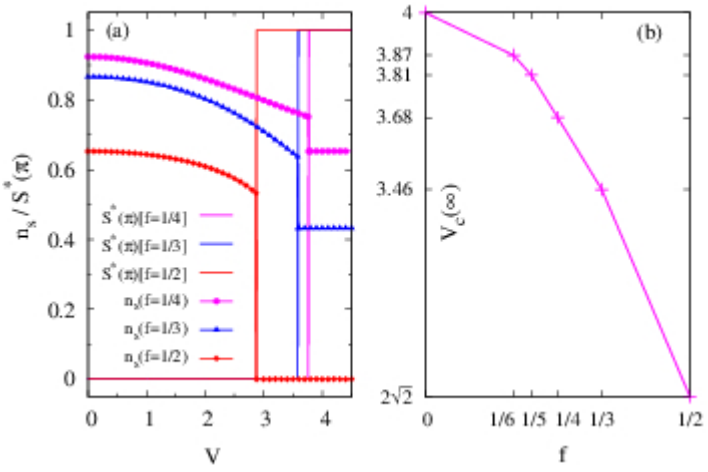

FIG. 3. (a) Plots of rescaled structure factor $\mathbf{S^*(\pi)}$ and superfluid fraction $\mathbf{n_s}$ at various filling factors **f** obtained using modified Lanczos technique. The calculations were at $\mathbf{f = 1/2, 1/4}$ with system size $\mathbf{N_s = 16}$ and at $\mathbf{f = 1/3}$ with $\mathbf{N_s = 12}$. At a critical repulsion there is a striking discontinuous transition; while $\mathbf{S^*(\pi)}$ jumps from its minimum to maximum, there is a significant

drop in $\mathbf{n_s}$. (b) Plot of $\mathbf{V_c(\infty)}$ (critical repulsion for an infinite system) obtained from Green's function analysis for half-filled ($\mathbf{f = 1/2}$) and two-HCB systems ($\mathbf{f \to 0}$) and from finite size scaling at various other fillings **f**.

A.3) Study of long-range orders of hard-core bosons coupled to cooperative normal modes in two-dimensional lattices.
Amrita Ghosh and Sudhakar Yarlagadda, arXiv:1610.01447

We study the possible manifestations of long-range orders, including lattice-supersolid phases with differently broken symmetry, in a two-dimensional square lattice system of HCBs coupled to archetypal cooperative/coherent normal-mode distortions such as those in perovskites. At strong HCB-phonon coupling, using a duality transformation, we obtain an effective Hamiltonian $\mathbf{t_1\text{-}t_2\text{-}t_3\text{-}V_1\text{-}V_2\text{-}V_3}$ involving nearest-neighbor, next-nearest-neighbor, and next-to-next-nearest-neighbor hoppings and repulsions. Using stochastic series expansion quantum Monte Carlo, we construct the phase diagram of the system. As coupling strength is increased, we find that the system undergoes a first-order quantum phase transition from a superfluid to a checkerboard solid at half filling and from a superfluid to a diagonal striped solid [with crystalline ordering wavevector $\mathbf{Q} = (2\pi/3, 2\pi/3)$ or $(2\pi/3, 4\pi/3)$] at one-third filling without showing any evidence of supersolidity. On tuning the system away from these commensurate fillings, checkerboard supersolid is generated near half filling whereas a rare diagonal striped supersolid is realized near one-third filling. Interestingly, there is an asymmetry in the extent of supersolidity about one-third filling. We identify the $\mathbf{t_1\text{-}V_1\text{-}V_2\text{-}V_3}$ model as the minimum model for obtaining a diagonal striped supersolid on a square lattice. Within our framework, we also provide an explanation for the observed checkerboard and diagonal-stripe formations in $\mathbf{La_{2-x}\,Sr_xNiO_4}$ at $\mathbf{x=1/2}$ and $\mathbf{x=1/3}$.

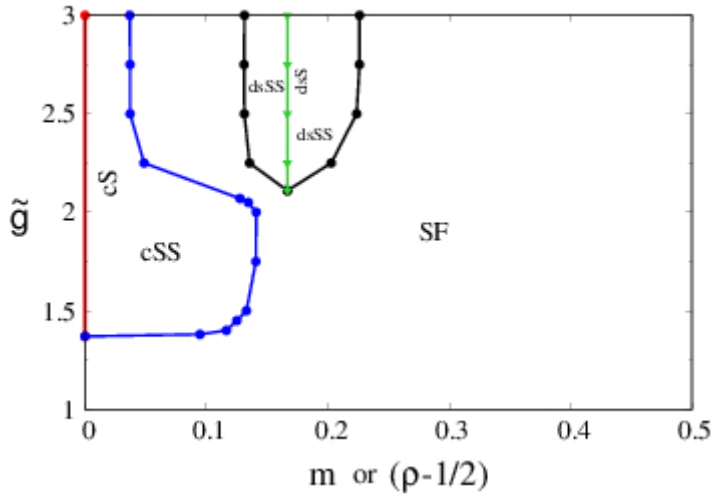

FIG. 4. Phase diagram in terms of magnetization (or filling-fraction ρ and HCB-phonon coupling for HCBs on a 18X18 lattice with adiabaticity $t/\omega_0 = 1.0$. cS represents checkerboard solid with **cSS** being the corresponding supersolid; dsS stands for diagonal striped solid with **dsSS** being the related supersolid. Plots represent averaged results from simulations employing three different random number seeds.

A.4) Correlated singlet phase in the one-dimensional Hubbard-Holstein model
Sahinur Reja, Sudhakar Yarlagadda, Peter B. Littlewood, Phys. Rev. B **86**, 045110 (2012).

A wealth of materials show evidence of strong electron-phonon (e-ph) interactions besides the ubiquitous electron-electron (e-e) interactions. For instance, transition metal oxides such as cuprates and manganites and molecular solids such as fullerides indicate strong e-ph coupling **g**. The interplay of e-e and e-ph interactions in these correlated systems leads to coexistence of or competition between various phases such as superconductivity, CDW, etc.

We derived an effective Hamiltonian for the one-dimensional Hubbard-Holstein model (using our duality treatment) and obtained the phase diagram at various fillings. As e-e interaction is increased, the system transits from an antiferromagnetic cluster to a correlated nearest-neighbor singlet phase (see figure below). We have analyzed the correlated nearest-neighbor singlet phase predicted by the effective Hamiltonian of the Hubbard-Holstein model by essentially mapping the Hamiltonian onto the well-understood one-dimensional $\mathbf{t_1}$-$\mathbf{V_1}$ model with large repulsion. Because the physics is dictated by the $\mathbf{t_1}$-$\mathbf{V_1}$ model, we find that CDW and superfluidity occur mutually exclusively with CDW resulting only at $\mathbf{n = 1/3}$ while superfluidity manifests itself at all other fillings. We also show that the BEC occupation number $\mathbf{n_0}$ for our model scales similarly to the $\mathbf{n_0}$ of a HCB-tight-binding model; additionally, we demonstrate numerically (using our new world-line QMC method and a modified Lanczos algorithm), at $\mathbf{n = 1/3}$, that the $\mathbf{n_0}$ for our model is smaller than the $\mathbf{n_0}$ for a HCB tight binding model.

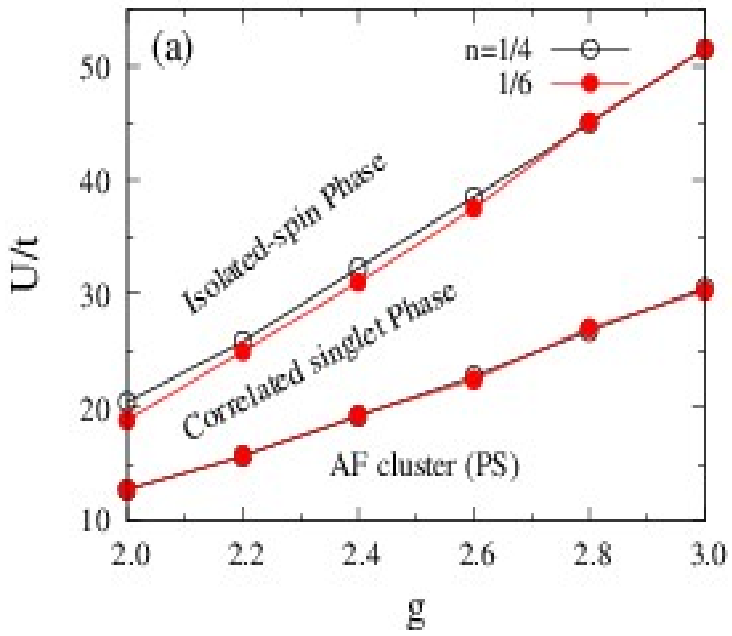

FIG. 5. Plots obtained using modified Lanczos in a twelve-site system for $\mathbf{t/\omega_0 = 1.0}$. Phase diagram (at various dimensionless e-e interactions **U/t** and e-ph couplings **g**) depicts that the phase transition lines are close for both densities $\mathbf{n = 1/4}$ and $\mathbf{n = 1/6}$.

B) Using strong-weak duality to analyze systems with strong cooperative electron-phonon interaction

The last few decades have witnessed numerous studies to fathom the tapestry of exotic phenomena

(such as long-range orderings) and interesting functionalities (such as colossal magnetoresistance, multiferroicity, superconductivity, etc.) in bulk transition metal oxides (such as the manganites, cuprates, etc.) and their interfaces. To model the emergent ordering and functionality in these complex metal oxides (and guide material synthesis), one needs, as building blocks, effective Hamiltonians for various interactions. Except for the cooperative electron-phonon interaction (EPI), effective Hamiltonians, that reasonably mimic the physics, have been derived for all other interactions. For instance, double exchange model approximates infinite Hund's coupling, Gutzwiller approximation or dynamical mean-field theory model Hubbard on-site Coulombic interaction, superexchange describes localized spin interaction at strong on-site repulsion, etc. Many oxides such as cuprates, manganites, and bismuthates indicate cooperative strong EPI.

B.1) Study of cooperative breathing-mode in molecular chains

Ravindra Pankaj and Sudhakar Yarlagadda, Phys. Rev. B **86**, 035453 (2012)

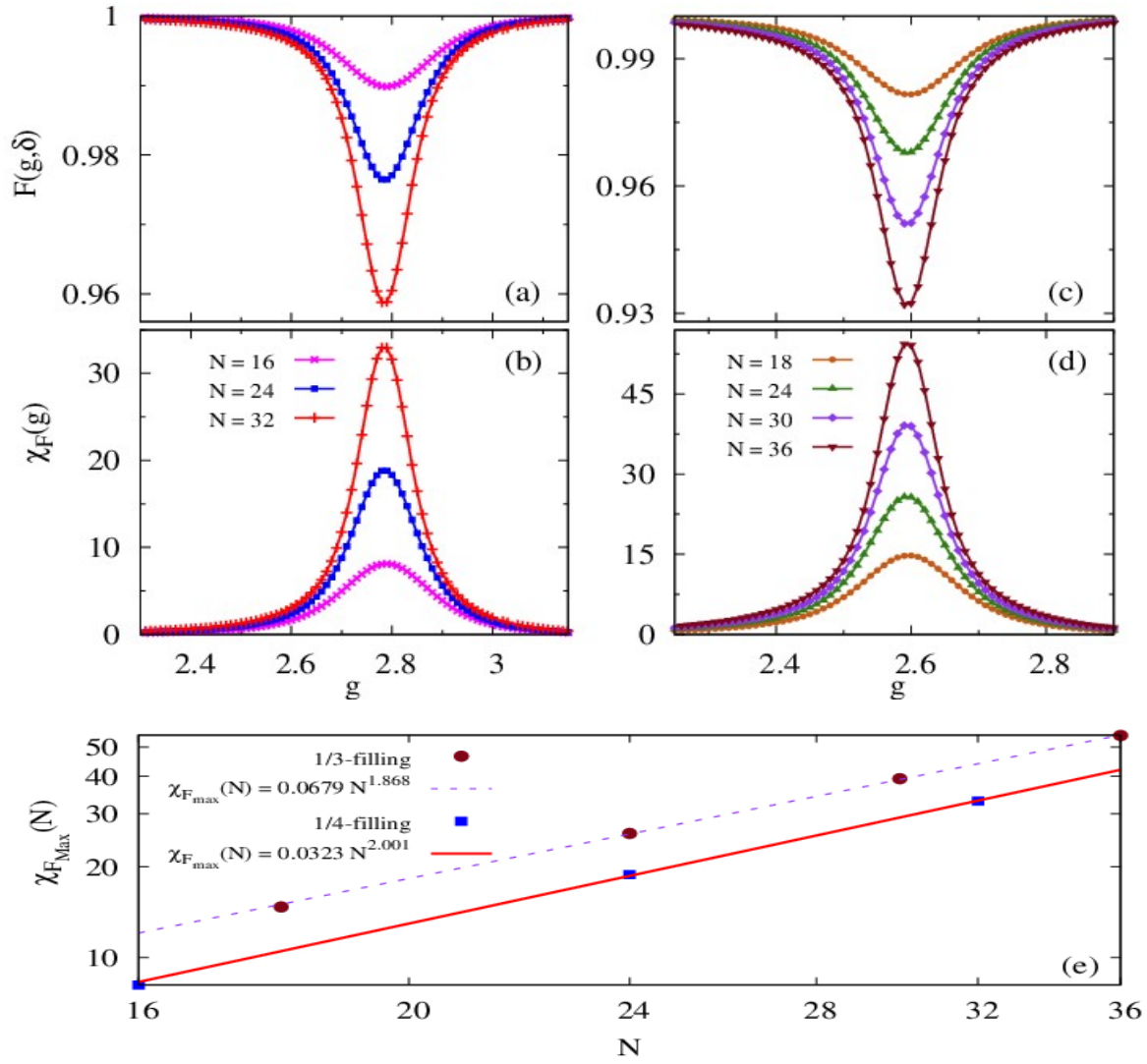

FIG. 11. Ground state fidelity (**GSF**) **F (g,δ)** in the CBM model at adiabaticity $\mathbf{t/\omega_0 = 0.1}$ and $\boldsymbol{\delta = 0.05}$ for (a) **1/4** filling and (c) **1/3** filling. Fidelity susceptilbility (**FS**) $\boldsymbol{\chi_F(g)}$ for (b) **1/4** filling and (d) **1/3** filling correspond to the **GSF** plots in (a) and (c). (e) Plot of the peak values of **FS** $\boldsymbol{\chi_{Fmax}(N)}$ versus **N**, on a logarithmic scale, at **1/4** filling and **1/3** filling and the corresponding power-law fits.

Many oxides that have the formula **ABO_3** assume a perovskite structure where two adjacent **BO_6** octahedra share an oxygen which leads to cooperative octahedral distortions. Understanding the cooperative electron-phonon phenomena in systems such as the bismuthates, the cuprates, and the manganites is still an open question. Using a controlled analytic nonperturbative treatment (involving a duality transformation) that accounts for the quantum nature of the phonons, we derive a model that generically describes the cooperative breathing-mode (CBM) at strong electron-phonon interaction in one-band one-dimensional systems [PRB **86**, 035453]. The effective model involves a next-nearest-neighbor hopping (that dominates over the nearest-neighbor hopping at strong coupling) and a nearest-neighbor repulsion that is significantly enhanced due to incompatibility of neighboring dilations/compressions. At non-half-filling, upon tuning the electron-phonon coupling, the system undergoes a period-doubling second-order quantum phase transition from a Luttinger liquid to a conducting commensurate charge-density-wave state: a phenomenon absent in both the Holstein model and the t_1-V_1 model. Using fidelity to study the nature of the quantum phase transition, we find that the fidelity susceptibility shows a superextensive power law divergence as well as a remarkable scaling behavior; both together establish a second-order transition (see figures above).

B.2) Charge and orbital order due to cooperative Jahn-Teller effect in manganite chains.

Ravindra Pankaj, Sudhakar Yarlagadda, arXiv:1608.06055

We derive an effective Hamiltonian that takes into account the quantum nature of phonons and models cooperative Jahn-Teller effect in the adiabatic regime and at strong electron-phonon coupling in one dimension. Our approach involves mapping a strong-coupling problem to a weak-coupling one by using a duality transformation. Subsequently, a sixth-order perturbation theory is employed in the polaronic frame of reference where the small parameter is inversely (directly) proportional to the coupling (adiabaticity). We study charge and orbital order in ferromagnetic manganite chains and address the pronounced electron-hole asymmetry in the observed phase diagram. In particular, at strong coupling, we offer an explanation for the observed density dependence of the wavevector of charge modulation, i.e., wavevector is proportional to (independent of) electron density on the electron-doped (hole-doped) side of the phase diagram of manganites. We also provide a picture for the charge and orbital order at special fillings **1/2** , **1/3**, **1/4**, and **1/5**; while focusing on the ordering controversy at fillings **1/3** and **1/4**, we find that Wigner-crystal arrangement is preferred over bi-stripe order.

C) Oxide devices as replacement for semiconductor devices

Although semiconductors are the most widely used functional materials for electronic applications so far, nevertheless, semiconductor devices have some limitations: i) the characteristic length scales are sizeable so that further scaling down the existing system size is quite difficult; and ii) only the charge and spin degrees of freedom are utilized. On the other hand, owing to significantly smaller extent of the wavefunction, transition metal oxides can meet the miniaturization demands much better than semiconductors. Furthermore, oxides offer a vastly richer physics involving diverse spin, charge, lattice, and orbital correlations. Low-dimensional oxides present new opportunities for devices where these diverse correlations can be optimized by engineering many-body interactions, fields, geometries, disorder, strain, etc. Therefore, oxides may be viewed as one of the best candidates to replace semiconductors in future electronic devices.

C.1.1) Study of decoherence in models for hard-core bosons coupled to optical phonons
A. Dey, M. Q. Lone, and S. Yarlagadda, Phys. Rev. B **92**, 094302 (2015).

C.1.2) Polaron dynamics and decoherence in an interacting two-spin system coupled to an optical-phonon environment
Amit Dey and S. Yarlagadda, Phys. Rev. B **89**, 064311 (2014).

Understanding coherent dynamics of excitons, spins, or hard-core bosons (HCBs) has tremendous scientific and technological implications for quantum computation. Here, we study decay of excited-state population and decoherence in a two-site HCB model with site-dependent strong potentials and subject to non-Markovian dynamics. The model is investigated in the regimes of antiadiabaticity and strong HCB-phonon coupling with each site providing a different local optical phonon environment; furthermore, the HCB system is taken to be initially uncorrelated with the environment in the polaronic frame of reference. We show clearly that the degree of decoherence and decay of excited state are enhanced by the proximity of the site-energy difference to the eigenenergy of phonons and are most pronounced when the site-energy difference is at resonance with twice the polaronic energy; additionally, the decoherence and the decay effects are reduced when the strength of HCB-phonon coupling is increased.

The model Hamiltonian is given by

$$H = \varepsilon_1(n_1 - 1/2) + \varepsilon_2(n_2 - 1/2) - J_\perp/2\,(b^\dagger_1 b_2 + b^\dagger_2 b_1) + J_\parallel\,(n_1 - 1/2)\,(n_2 - 1/2) + g\omega \sum_{i=1,2}(n_i - 1/2)(a_i + a^\dagger_i) + \omega \sum_{i=1,2}(a^\dagger_i a_i) \qquad (2)$$

where ε_1 and ε_2 are the site energies, $J_\perp/2$ (>0) is the hopping, and $J_\parallel$ (>0) is the repulsion strength between HCBs on the adjacent sites.

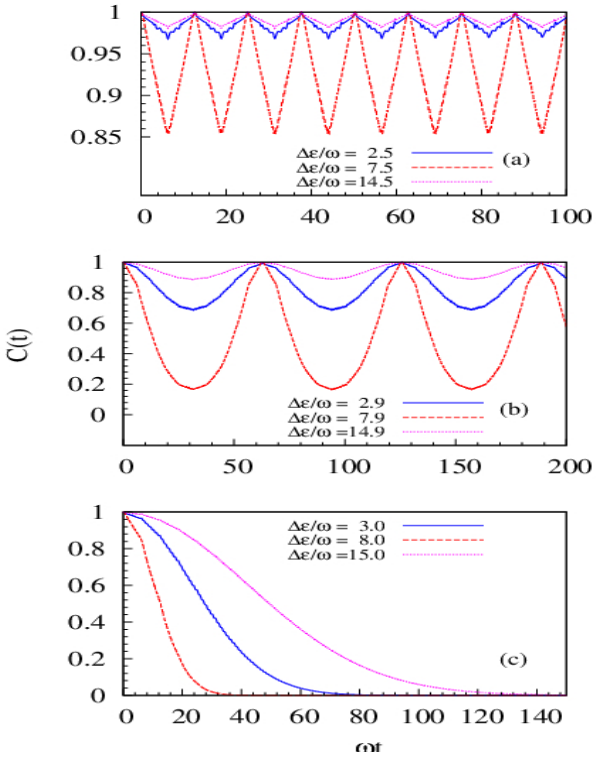

FIG. 6. Time (ωt) dependence of **C(t)** for $J_\perp/\omega = 0.5$, **g=2.0**, and when (a) $\Delta\varepsilon/\omega$ = **2.5**, **7.5**, and **14.5**; (b) $\Delta\varepsilon/\omega$ = **2.9**, **7.9**, and **14.9**; and (c) $\Delta\varepsilon/\omega$ = **3.0**, **8.0**, and **15.0**.

In the two-site HCB model, the dynamics of population as well as the coherence are important for understanding physical systems such as a double quantum dot (DQD) acting as a qubit for quantum computation. An oxide- (i.e., manganite-) based DQD, with appropriate detuning, can serve as a charge qubit with very small decoherence compared to a semiconductor DQD; furthermore, it can also meet the demands of miniaturization as its size can also be much smaller than a semiconductor DQD.

C.2) Temperature dependence of long coherence times of oxide charge qubits.
A. Dey, S. Yarlagadda, arXiv:1610.01866

K_BT/ω_u	$\Delta\varepsilon/\omega_u$ = 0.0	0.2	0.5	0.8
0.01	>100 s	>100 s	>100 s	>100 s
0.15	50 ps	24 μs	> 0.1 s	83 ns
0.50	1 ps	47 ps	0.75 μs	10 ps

TABLE. I. Coherence times at various values of scaled thermal energy K_BT/ω_u and detuning energy $\Delta\varepsilon/\omega_u$ when optical phonon energy $\omega_u = 0.05$ eV.

The ability to maintain coherence and control in a qubit is a major requirement for quantum computation. We show theoretically that long coherence times can be achieved above boiling point of liquid helium in charge qubits of oxide double quantum dots. Detuning the dots to a fraction of the optical phonon energy, increasing the electron-phonon coupling, reducing the adiabaticity, or decreasing the temperature enhances the coherence time. We consider a system that is initially decoupled from the phonon bath in the polaronic frame of reference and solve the non-Markovian quantum master equation; we find that the system decoheres after a long time, despite the fact that no energy is exchanged with the bath.

C.3) Giant magnetoelectric effect in pure manganite-manganite heterostructures.
Sanjukta Paul, Ravindra Pankaj, Sudhakar Yarlagadda, Pinaki Majumdar, Peter B. Littlewood, arXiv:1702.06302

Obtaining strong magnetoelectric couplings in bulk materials and heterostructures is an ongoing challenge. We demonstrate that manganite heterostructures of the form

(Insulator)/$(LaMnO_3)_n$/Interface/$(CaMnO_3)_n$/(Insulator)

show strong multiferroicity in magnetic manganites where ferroelectric polarization is realized by

charges leaking from $LaMnO_3$ to $CaMnO_3$ due to repulsion. Here, an effective nearest-neighbor electron-electron (electron-hole) repulsion (attraction) is generated by cooperative electron-phonon interaction. Double exchange, when a particle virtually hops to its unoccupied neighboring site and back, produces magnetic polarons that polarize antiferromagnetic regions. Thus a striking giant magnetoelectric effect ensues when an external electrical field enhances the electron leakage across the interface.

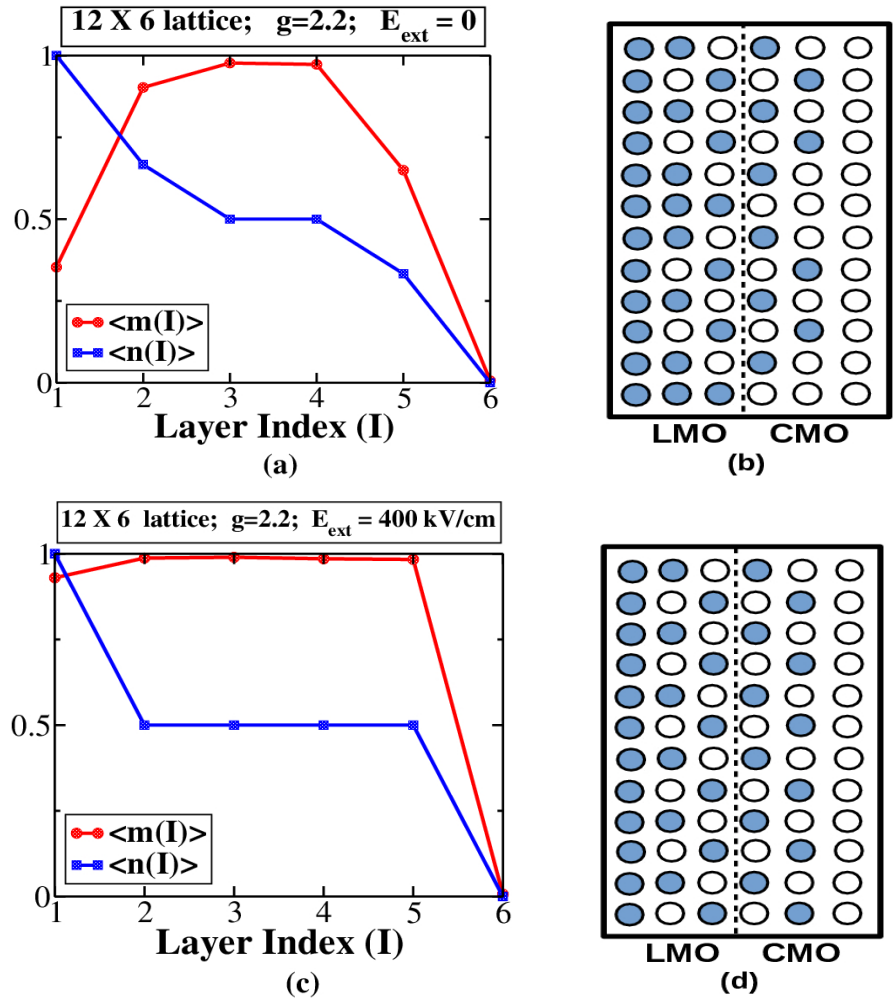

FIG. 7. In a symmetric **12X6** lattice, for coupling **g = 2.2**, (a) at zero electric field, layer-averaged charge density **<n(I)>** and layer-averaged magnetization **<m(I)>** of t_{2g} spins normalized to unity; (b) at $E_{ext} = 0$, ground state configuration; (c) at strong external electric field $E_{ext} = 400$ **V/cm**, layer-averaged charge density **<n(I)>** and layer-averaged magnetization **<m(I)>** of t_{2g} spins normalized to unity; and (d) at $E_{ext} = 400$ **kV/cm**, charge configuration in the ground state.

D) Correlation between battery material performance and cooperative electron-phonon interaction in $LiCo_yMn_{2-y}O_4$

K. Ragavendran, P. Mandal, and S. Yarlagadda, Appl. Phys. Lett. **110**, 143901 (2017).

So far designing new battery materials has been based on intuition and chemical concepts. However, it is highly essential to couple these efforts with basic physics (experimental and theoretical) investigations so that better batteries can be designed. Despite the fact that battery

materials show striking similarities with the perovskite manganites and sodium cobaltate, problems in battery materials are hardly addressed by the physics community. The present work establishes the much-needed correlation between battery performance and basic physics pertaining to battery material (such as $LiCo_yMn_{2-y}O_4$). It is believed that the present study will provide a new insight into designing Li-ion battery cathodes and stimulate further research activity, along similar directions, among the physicists.

The relation between electrochemical performance, activated-transport parameters, thermal expansion, and cooperativity of electron-phonon-interaction distortions in $LiCo_yMn_{2-y}O_4$ is investigated. The first order cooperative-normal-mode transition, detected through coefficient of thermal expansion, is found to disappear at a critical doping (**y ~ 0.16**); interestingly, for **y ≳0.16** the resistivity does not change much with doping and the electrochemical capacity becomes constant over repeated cycling. The critical doping **y ~ 0.16** results in breakdown of the network of cooperative/coherent normal-mode distortions; this leads to vanishing of the first-order transition, establishment of hopping channels with lower resistance, and enhancing lithiation and delithiation of the battery, thereby minimizing electrochemical capacity fading.

The resistivity in $LiCo_yMn_{2-y}O_4$ can be expressed as follows

$$\rho = [A \exp(2R/\xi)/n] \exp(E_a/K_BT) \qquad (3)$$

A is a constant, **n** is the concentration of the e_g electrons, ξ is the localization length, **R** is the shortest hopping distance for an e_g electron (i.e., the distance between two neighboring Mn^{3+} and Mn^{4+} ions), and **T** is the temperature. Even upon doping with cobalt (where Co^{3+} replaces Mn^{3+}), each Mn^{3+} has the same number of diagonally opposite Mn^{4+} ions for the e_g electron to hop to; this justifies using a fixed-hopping-distance model rather than a variable-hopping-range model.

FIG. 8. Linearity in plots of $\log_{10}(\rho)$ vs $1/T$ depicting activated transportat various dopings and above the structural transition. For doping below **y ~ 0.16**, the resistivity drops sizeably with increase in doping; contrastingly, for **y ≳0.16**, the resistivity does not change much with doping.

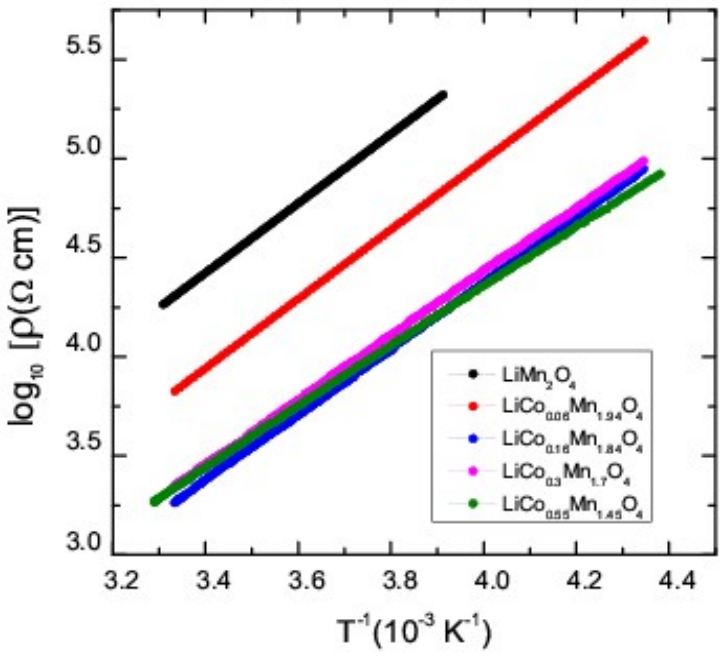

Our transport model is clearly verified by Fig. 8 which depicts linear plots of $\log_{10}(\rho)$ versus $1/T$. Using Fig. 8, at various Co-doping values, we extract the prefactor $A\exp(2R/\xi)/n$ and the activation energy E_a [occurring in Eq. (3)] and generate Fig. 9. Now, the cobalt doping has two competing effects on the localization length ξ: (i) the frustration (produced by electron-electron repulsion) decreases with increase in doping and, thus, tends to increase ξ; (ii) contrastingly, the disorder effect due to doping tends to decrease ξ. However, at a critical doping y_c, there is a breakdown of the cooperative normal-mode-network and frustration is no longer significant to ξ for dopings beyond y_c. Thus, above $y \sim y_c$, ξ decreases with increasing doping; on the other hand, below $y \sim y_c$, ξ increases rapidly with doping. Furthermore, $1/n$ increases gradually with doping. Hence, in the above expression for resistivity, the prefactor $A\exp(2R/\xi)/n$ will have a minimum as a function of Co-doping. In fact, as depicted in Fig. 9, the minimum in the prefactor $A\exp(2R/\xi)/n$ occurs at $y \sim 0.16$ which leads us to estimate $y_c \sim 0.16$. Lastly, it is of interest to note that the resistivity drops sizeably with increasing doping until the doping-level attains a value $y \sim 0.16$; at higher doping values (i.e., $y \gtrsim 0.16$), the resistivity does not change much (as can be seen in Fig. 8). This can be understood in terms of a non-cooperative network being established at $y = y_c \sim 0.16$; above y_c, in Eq. (3) for resistivity, an increase in the prefactor $A\exp(2R/\xi)/n$ is compensated by a reduction in $\exp(E_a/K_BT)$.

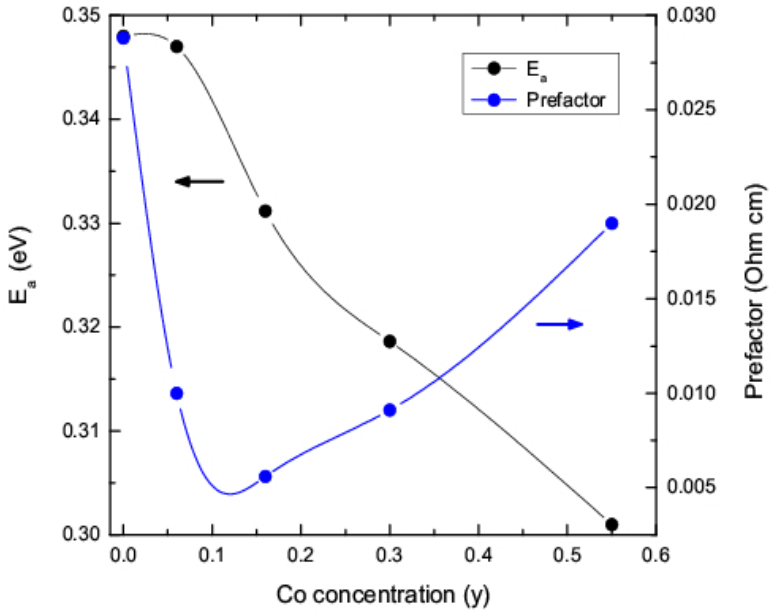

FIG. 9. Plots of the prefactor $A\exp(2R/\xi)/n$ and the activation energy E_a [occurring in the resistivity equation (3)] as a function of cobalt doping in $LiCo_yMn_{2-y}O_4$. The prefactor shows a minimum at $y \sim 0.16$ and the drop in E_a is sharper till $y \sim 0.16$; both are indicative of a change in the transport mechanism.

Finally, we will discuss capacity fading as displayed in Fig. 10. In the undoped case and at lower dopings (i.e., $y < 0.16$), the network of cooperative/coherent normal-mode distortions restricts

lithiation (delithiation) of the cathode material; consequently, each time only a fraction of the un-lithiated (lithiated) material gets lithiated (delithiated). On increasing the doping to $\mathbf{y \gtrsim 0.16}$, a network of non-cooperative normal-mode distortions is established which facilitates both the lithiation and the delithiation processes. Thus, while there is capacity fading upon repeated cycling at lower values of doping (i.e., $\mathbf{y < 0.16}$), the capacity remains constant for $\mathbf{y \gtrsim 0.16}$. However, for $\mathbf{y \gtrsim 0.16}$, at higher doping values the capacity is less due to decrease in the number of $\mathbf{e_g}$ carriers. Thus ideally, it is best to use $\mathbf{LiCo_yMn_{2-y}O_4}$ at $\mathbf{y \sim 0.16}$ for optimal electrochemical performance.

FIG. 10. Variation of the capacity as a function of cycle number for $\mathbf{Li/LiCo_yMn_{2-y}O_4}$ cells at various cobalt dopings. At higher doping $\mathbf{y \sim 0.16}$, capacity remains unchanged after repeated cycling. Reproduced with permission from J. Electrochem. Soc. **145**, 807 (1998).

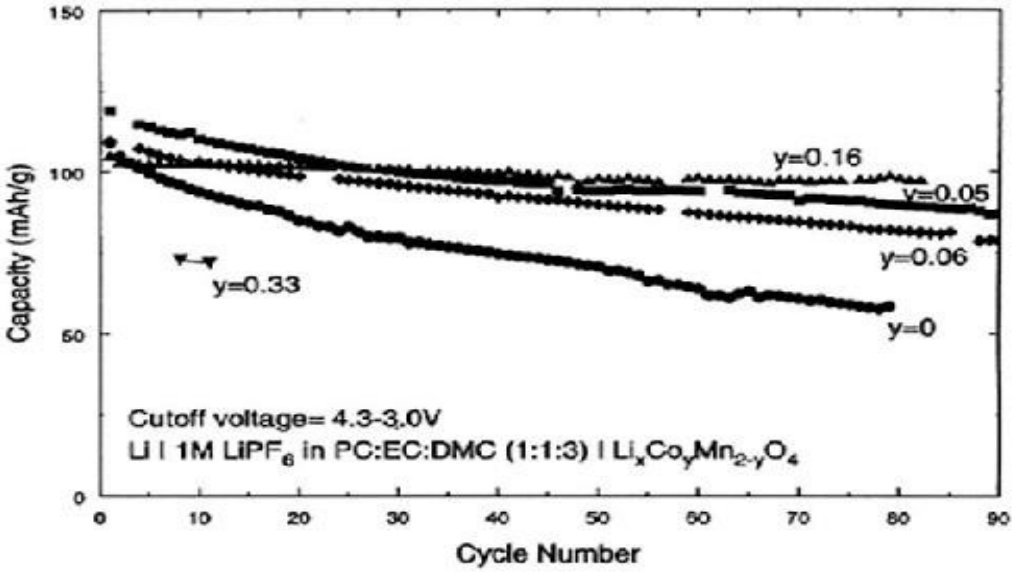

E) Study of two-spin entanglement in singlet states

M. Q. Lone, A. Dey, and S. Yarlagadda, Solid State Communications **202**, 73 (2015).

Valence-bond (VB) states were shown to be the ground states of spin systems earlier by C. K. Majumdar's group and later by Shastry and Sutherland. Any spin-singlet state (i.e., state with total spin eigenvalue $\mathbf{S_T = 0}$) can be expressed as a superposition of VB states. Correlation/entanglement between two spins plays an important role in understanding phase

transitions, length scale in the system, etc. Although two-spin correlation/entanglement has been investigated in certain Resonating-valence-bond (RVB) states, to our knowledge, there has been no explicit construction of RVB states that would contain maximal entanglement of two-spin subsystems.

The spins of a two-spin singlet, while being maximally entangled with each other, are completely unentangled with the remaining spins and thus show monogamy. Thus, if we wish to establish greater entanglement between the two-spin subsystem and the rest of the spin system, we are forced to diminish entanglement between the spins of the two-spin subsystem. The purpose of this work is to enhance our understanding of the distribution of two-spin entanglement in singlet states. We analyze the following two extreme cases in a general singlet: (1) maximal average entanglement between two spins; and (2) maximal average entanglement between a two-spin subsystem and the remaining spins. The main results of this work are as follows. First, we study two-spin entanglement in singlets. We show that the average entanglement between two spins is maximum (as expected) for a single VB state. In a singlet, we also demonstrate that **SU(2)** isotropy and homogeneity (in spin-spin correlation function) maximize the bipartite entanglement $\mathbf{E^2_v}$ (the average entanglement between a subsystem of two spins and the rest of the system) while minimizing the average entanglement between two spins. Second, we adopt two ways of obtaining maximal $\mathbf{E^2_v}$ states: (1) imposing homogeneity on singlet states; and (2) generating isotropy in a general homogeneous state. By using these two approaches, we construct explicitly four-spin and six-spin highly entangled states that are both isotropic and homogeneous. Our maximal $\mathbf{E^2_v}$ states represent a new class of RVB states which we show to be the ground states of the infinite-range Heisenberg model.